Robust 3D segmentation of anatomical structures with level sets

C. Baillard and C. Barillot

IRISA, Campus de Beaulieu, 35042 Rennes cedex, France

{Caroline.Baillard,Christian.Barillot}@irisa.fr

Abstract

This paper is focused on the use of the level set formalism to segment anatomical structures in 3D images (ultrasound ou magnetic resonance images). A closed 3D surface propagates from an initial position towards the desired boundaries through the iterative evolution of a 4D implicit function. The major contribution of this work is the design of a robust evolution model which does not require a fine tuning of a set of parameters. It involves adaptive parameters depending on the data and on the current state of the process. The iteration step and the external propagation force, both usually constant, are automatically computed at each iteration. In addition, region-based information rather than gradient is used, via an estimation of intensity probability density functions over the image. As a result, the method can be applied to very different kinds of data. Results on brain MR images and 3D echographies of carotid arteries are presented and discussed.

key words: 3D segmentation, deformable models, level sets, intensity statistical analysis, probability density functions, brain MRI, 3D ultrasound.

1 Introduction

The 3D segmentation of anatomical structures has become crucial for many medical applications, both for visualization and clinical diagnosis purposes. Due to the huge amount of data and the complexity of anatomical structures, manual segmentation is extremely tedious and often inconsistent. Automatic segmentation methods are required to fully exploit 3D data. It is a very challenging task because they can not usually rely on image information only. Anatomical tissues are generally not homogeneous and their boundaries are not clearly defined in the images. It is therefore often necessary to involve *a priori* knowledge about the shape or the radiometric behaviour of the structure of interest.

Deformable models define a powerful tool to accurately recover a structure using very few assumptions about its shape [13]. Such a model iteratively evolves towards the desired location according to a global energy minimization process. The functional energy is based on external forces derived from the data and internal forces related to the geometry of the contour. The limitations of this approach are well-known: the contour must be initialized close to the desired boundaries, and it can not cope with significant protusions nor topological changes. In the last few years, segmentation methods based on level sets have become very popular because they overcome classical limits of deformable models [9, 7, 2]. The evolving surface can change topology and cope with complex geometry, and the result is

less dependent on initialization than with any other iterative method. This kind of approach has already been applied within a wide range of applications in computer vision. However, parametrization is still a limitation for practical use. Several evolution models have been proposed, but most of them include many parameters to be tuned: iteration step, weighting parameters, constant propagation term, etc. The tuning of these parameters determines the success of the method.

This paper describes a robust evolution model. It enables a volume to be segmented with almost no parameter setting. It relies on adaptive parameters depending on the data and on the current state of the process. In addition, region-based information rather than gradient is utilized, via an estimation of intensity probability density functions over the image. The versatility of the segmentation is demonstrated on both brain structures in MR images and carotid arteries in 3D echography. Our strategy is presented in section 2. The two main stages of the method - intensity distribution analysis and surface evolution - are described in sections 3 and 4. Experimental results are presented and discussed in section 5.

2 Segmentation strategy based on level sets

Within the level set formulation [9], the evolving surface $S(t)$ is processed as a propagating front embedded as the zero level of a 4D scalar function $\Psi(\mathbf{x}, t)$. This hypersurface is usually defined as the signed distance from $\mathbf{x}$ to the front S (negative *inside* the object). The evolution rule for Ψ is:

$$\frac{\partial \Psi}{\partial t} + F|\nabla \Psi| = 0, \tag{1}$$

where F is a scalar *velocity function* depending on the local geometric properties of the front (local curvature) and external parameters related to the input data (image gradient for instance). The hypersurface Ψ deforms iteratively according to F, and the position of the 3D front $S(t)$ is deduced from Ψ at each iteration step using the relation $\Psi(\mathbf{x}(t), t) = 0$. Practically, the hypersurface Ψ^{n+1} at step $n+1$ is computed from Ψ^n at step n using the relation:

$$\Psi^{n+1}(\mathbf{x}) = \Psi^n(\mathbf{x}) - \Delta t.F|\nabla \Psi^n(\mathbf{x})|, \quad \forall \mathbf{x} \in I\!R^3 \tag{2}$$

The design of the velocity function F plays the major role in the evolution process. Several formulations have been proposed [4, 2, 11, 15]. We have chosen the original formulation given by Malladi et.al. [7] for its simplicity:

$$F = h_I(\nu + \rho\kappa) \tag{3}$$

The term ν represents an external propagation force which makes the surface contract or expand. The parameter κ represents the local curvature of the front and acts as a regularization term. The weighting ρ expresses the importance given to regularization. Finally, the term h_I is the data consistency term: it depends on the intensity I of the input data, and acts as a stopping criterion at the location of the desired boundaries by taking a small value.

In the following, our definition of the parameters introduced in equations (2) and (3) is presented. They require the intensity probability density functions (PDFs) inside and outside the structure to be known. These PDFs will be respectively denoted $p_i(I)$ and $p_e(I)$, and the *a priori* probability for a voxel to be *inside* the structure will be denoted α_i. Our general strategy is illustrated in figure 1. The PDFs are first estimated by using both the initial segmentation and given statistical distribution models. This allows the parameters of the velocity function to be computed for the evolution of the hypersurface. If the PDFs can not be accurately approximated with the input models, the estimates can be updated at each iteration using the current segmentation. The two stages are further described in the next two sections.

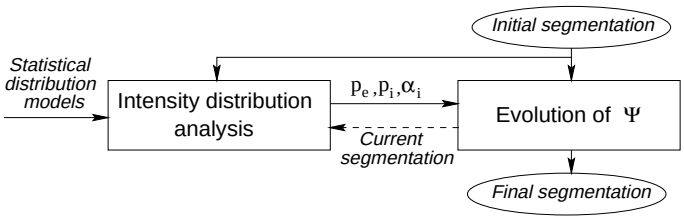

Figure 1: *Strategy for 3D segmentation. The velocity function controlling the surface evolution is computed according to the estimated intensity density functions inside and outside the structure.*

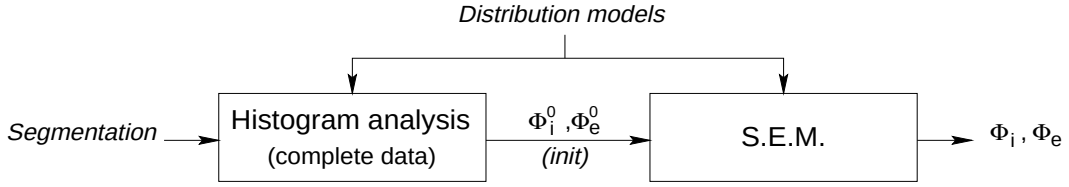

Figure 2: *Estimation of the mixture model parameters (Φ_I inside the object and Φ_e outside the object), when the distribution is bimodal.*

3 Estimation of intensity Probability Density Functions

In this work, it is assumed that the intensity distribution over the image is bimodal, i.e., the object to be segmented and its background can both be approximated by a specific monomodal distribution. This is true for many images, for instance the 3D ultrasound images of carotid artery shown in figures 5 and 6. If a bimodal distribution is not realistic (like for brain MR images), one solution is to use mixture estimation methods [8, 12]. However, the approximation of the inner and outer distributions by two Gaussian models has given satisfactory results within our experiments. Let us denote Φ_i and Φ_e the parameter vectors of the bimodal distribution mixture, respectively characterizing the interior and the exterior of the structure of interest (they entirely determine p_i, p_e and α_i). Given a coarse segmentation of the structure, two independent histograms are produced from the data (one for the structure and one for its background). The variables Φ_i and Φ_e are independently estimated over these complete data, providing two coarse parameter estimates Φ_i^0 and Φ_e^0.

Two cases have been then distinguished. If the distribution mixture is bimodal, the parameters Φ_i^0 and Φ_e^0 initialize a Stochastic Expectation-Maximisation (SEM) algorithm. This approach is illustrated in figure 2. The SEM algorithm does not guarantee the optimal solution, but in practice any initial partition roughly representative of the inner and the outer distribution leads to the correct solution. In particular, the initial surface used for the estimation of Φ_i^0 and Φ_e^0 does not need to be close to the real boundaries. If the segmentation must be initialized with a very small volume inside the object, a rough segmentation can be first produced with a classical model of velocity function (stopping function h_I based on image gradients and constant external propagation force ν). Figure 3 shows an example of PDFs computed with this method.

If the distribution is not bimodal, the SEM algorithm can not be applied. In this case, the *prior* α_i is initialized to 0.5 and updated by stochastic estimation. The resulting vectors Φ_i and Φ_e are used for computing the velocity function, but they are updated at each iteration using the current segmentation. Although convergence is not theorically guaranteed, the process appears to be very stable for MR images. In both cases, an estimation of the PDFs p_i, p_e and of the *prior* α_i is available at any time of the process.

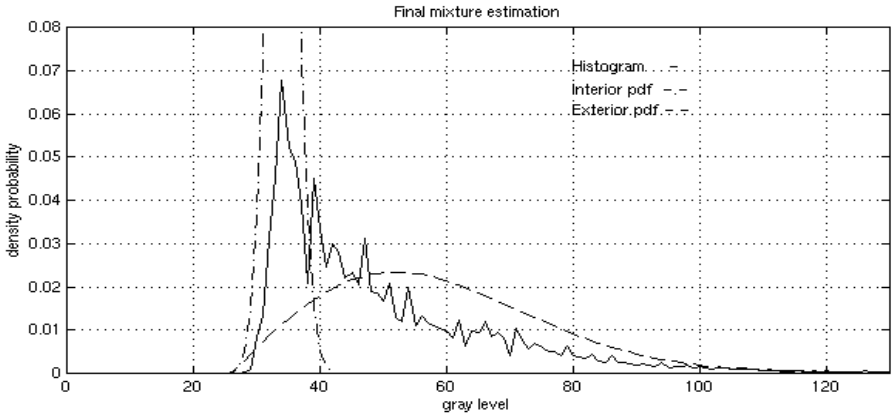

Figure 3: *Exemple of estimated mixture model (from the input data shown in figure 5).*

4 Evolution model

4.1 External propagation term ν

In equation (3), the sign of ν determines the direction of the external propagation force. Several approaches to 3D segmentation using this evolution model have imposed a one-way propagation force ν, which either contracts or expands the whole surface all along the process [6, 15]. However, when the initial position of the surface can be predicted (by tracking or by registration with an atlas for instance), the predicted and real positions usually overlap. It is therefore necessary to let the surface evolve in both directions. Some propagation models have been designed in order to solve this problem in 2D, by involving a local analysis of intensity [10, 1, 14].

The problem can be expressed as the classification of each point of the current interface $S(t)$. If a point belongs to the object then the surface should locally extend; if it does not, the surface should contract. We perform this classification by maximizing the *a posteriori* segmentation probability $p(\lambda|I)$, where $\lambda \in \{\lambda_i, \lambda_e\}$ denotes the appartenance class of the considered point ($\lambda = \lambda_i$ inside the object and $\lambda = \lambda_e$ outside the object). According to Bayes rule, the maximization of the posterior distribution $p(\lambda|I)$ is equivalent to the maximization of $p(\lambda)p(I|\lambda)$, where $p(\lambda)$ is the *prior* of the class λ ($p(\lambda_i) = \alpha_i$) and $p(I|\lambda)$ is the likelihood of intensity. The propagation term ν has then been defined as:

$$\nu = \text{Sign}\{\alpha_i p_i(I) - (1 - \alpha_i)p_e(I)\}. \tag{4}$$

When $p(\lambda_i|I) > p(\lambda_e|I)$, then $\nu > 0$. The point is more likely to be *inside* the object than *outside*, and the surface extends. Note, we always have $|\nu| = 1$. The respective roles of the propagation and the regularization terms are entirely determined by the weight ρ, which makes the process very easy to tune (more stability).

4.2 Curvature term $\rho\kappa$

The regularization parameter κ at a point $\mathbf{x}$ is the curvature of the interface, computed at the closest point to $\mathbf{x}$. This curvature is computed using the partial derivatives of Ψ:

$$\kappa_0 = \frac{(\Psi_{xx} + \Psi_{yy})\Psi_z^2 - 2\Psi_x\Psi_y\Psi_{xy} + (\Psi_{yy} + \Psi_{zz})\Psi_x^2 - 2\Psi_y\Psi_z\Psi_{yz} + (\Psi_{zz} + \Psi_{xx})\Psi_y^2 - 2\Psi_z\Psi_x\Psi_{zx}}{2(\Psi_x^2 + \Psi_y^2 + \Psi_z^2)^{1.5}}$$

The weighting parameter ρ can be interpreted as the particular curvature radius leading to a stable position ($F = 0$).

4.3 Data consistency term h_I

The data consistency term is traditionally related to the intensity gradient ∇I of the input image [7]. Since this gradient is only defined for points belonging to the interface (zero level set of the hypersurface), an *extended* gradient function need to be defined over $\mathbb{R}^3$ by the intensity gradient of the closest neighbour on the interface. However, gradient information has no meaning for very noisy and/or low-contrasted images (like ultrasound data). Besides, high gradients do not necessarily indicates a relevant boundary between the structure to be segmented and its background.

Similarly to the approach described in [11] for the 2D case, we have related this term to the *posterior* probability of having a transition between the object and its background. Let $\mathbf{x}$ be a voxel of the image, $\mathcal{N}$ a neighbourhood of $\mathbf{x}$ partitionned into 2 regions $\mathcal{N}_i$ and $\mathcal{N}_e$ respectively inside and outside the object, and $p_T(\mathbf{x}|I)$ the probability of $\mathbf{x}$ being a transition, given the observed intensity I :

$$p_T(\mathbf{x}|I) = p(\mathbf{x} \in S|I(\mathcal{N})) = \frac{p(I(\mathcal{N})|\mathbf{x} \in S)p(\mathbf{x} \in S)}{p(I(\mathcal{N}))}$$

Assuming the intensity values of $\mathcal{N}_i$ and $\mathcal{N}_e$ are independent, the conditional probability $p(I(\mathcal{N})|\mathbf{x} \in S)$ can be expressed as:

$$p(I(\mathcal{N})|\mathbf{x} \in S) = p(I(\mathcal{N}_i)|\mathcal{N}_i \subset V)p(I(\mathcal{N}_e)|\mathcal{N}_e \subset \bar{V}),$$

where V denotes the interior of the volume and $\bar{V}$ its complementary. As a result:

$$p_T(\mathbf{x}|I) = \frac{p_i(I(\mathcal{N}_i))}{p(I(\mathcal{N}_i))}\frac{p_e(I(\mathcal{N}_e))}{p(I(\mathcal{N}_e))}p_T(\mathbf{x}), \tag{5}$$

where $p_T(\mathbf{x}) = p(\mathbf{x} \in S)$ is the *prior* of having a transition at $\mathbf{x}$ (independent from the data). The estimation of the PDFs p, p_i and p_e has been explained in the previous section. The *prior* $p_T(\mathbf{x})$ is set to 0.5, which is a common assumption to model ignorance. Like in [11], the neighbourhood regions are $3 \times 3 \times 3$ windows. However, the partition $\{\mathcal{N}_i, \mathcal{N}_e\}$ is determined by the current normal vector $\mathbf{n} = \frac{\Delta\Psi}{|\Delta\Psi|}$.

The data consistency term h_I at a point $\mathbf{x}$ is finally defined as a decreasing function of the *posterior* transition probability $p_T(\mathbf{x}'|I)$ of the closest point on the current interface:

$$h_I(\mathbf{x}) = exp\{-k.p_T(\mathbf{x}'|I)\} \tag{6}$$

Practically, we choose $k = 1$ for all experiments.

4.4 Iteration step Δt

The iteration step Δt of equation (2) is usually constant and manually tuned. We propose to compute it automatically at each iteration in order to improve robustness.

The stability of the process requires a numerical scheme for the computation of $\Delta\Psi$, called *upwind sheme*. This scheme induces a limit on the iteration step Δt, called the CFL restriction (Courant-Friedrichs-Levy). More precisely, writing equation (1) as $\Psi_t + H(\Psi_x, \Psi_y, \Psi_z) = 0$, where H is the Hamiltonian defined by:

$$H(u, v, w) = \sqrt{u^2 + v^2 + w^2}.F, \tag{7}$$

the CFL restriction can be expressed in 3D [5] as:

$$1 \geq \Delta t.(\frac{|H_u|}{\Delta x} + \frac{|H_v|}{\Delta y} + \frac{|H_w|}{\Delta z}),$$

where H_u, H_v, H_w denote the partial derivatives of H with respect to u, v, w. Since we work with a regular sampling grid, we can assume $\Delta x = \Delta y = \Delta z = 1$. As a result, the maximal value for Δt which guarantees the stability of the numerical scheme is given by:

	0% noise, 0% inhom.			3% noise, 20% inhom.			9% noise, 40% inhom.		
	Sens.	Spec.	Total	Sens.	Spec.	Total	Sens.	Spec.	Total
Morpho maths	86.7%	98.7%	95.7%	83.5%	99%	95.2%	69.8%	99.5%	92.3%
Level sets	96.3%	98.9%	98.3%	95.1%	99.3%	98.2%	92.5%	99.2%	97.5%

Table 1: *Quantitative assessment on simulated data. Specificity, sensibility and total performance measures are given for 3 levels of noise and 2 segmentation methods.*

$$\tilde{\Delta t} = \min\{\frac{1}{|H_u| + |H_v| + |H_w|}\}$$

We propose to evaluate this value at each iteration of the process. According to equation (3) and the definition of the parameters involved, the velocity function F is independent from u, v, w. The terms h_I and ν only depends on the image data. The curvature term κ is the curvature of the interface at the closest point, and it does not depend on the local characteristics of Ψ. Therefore the partial derivatives of H can be directly computed from (7), and the best value for Δt which guarantees stability is given by:

$$\tilde{\Delta t} = \min\{\frac{\sqrt{u^2 + v^2 + w^2}}{(|u| + |v| + |w|)F}\} \tag{8}$$

5 Experimental results

5.1 Segmentation of brain MR images

Experiments have been run on a database of 18 MR images (volume size of $256 \times 256 \times 176$). Figure 4 shows the segmentation results on two different subjects. The weighting parameter ρ of eq. (3) has been set to 1, giving a very small importance to regularization. Protusions of brain and ventricles are properly recovered, despite of the surface being initialized far away from it. The method can naturally cope with change of topology: the ventricles inside the brain have also been recovered. On average, 850 iterations are necessary to segment the whole brain starting from a $40 \times 80 \times 80$ cube. The segmentation was also numerically assessed with simulated data provided by the MNI [3]. It was compared with a segmentation method based on morphological operators and tuned with a "best practice" parameter set. The results are summarized in table 1. The total performance achieved with our method varies between 98.3% and 97.5% in critical conditions (9% noise and 40% inhomogeneity), which is far better than the other method. A variational approach involving statistical models significantly improves the sensitivity and the robustness of the segmentation.

5.2 Segmentation of 3D ultrasound images

The method has also been applied to 3D ultrasound images of carotid artery. This kind of images is difficult to segment automatically due to the speckle noise. The intensity distribution inside the carotid has been modelized by a Gaussian (shadow area), whereas the exterior is modelized by a Rayleigh distribution (reverberation area) [8]. We have used a weighting value of $\rho = 10$ on regularization. All the other parameters have got the same value as for experiments on brain MRI. Figures 5 and 6 show the results of segmentation on two different images. They allow us to be very optimistic about the use of our statistical variational approach to segment 3D ultrasound images.

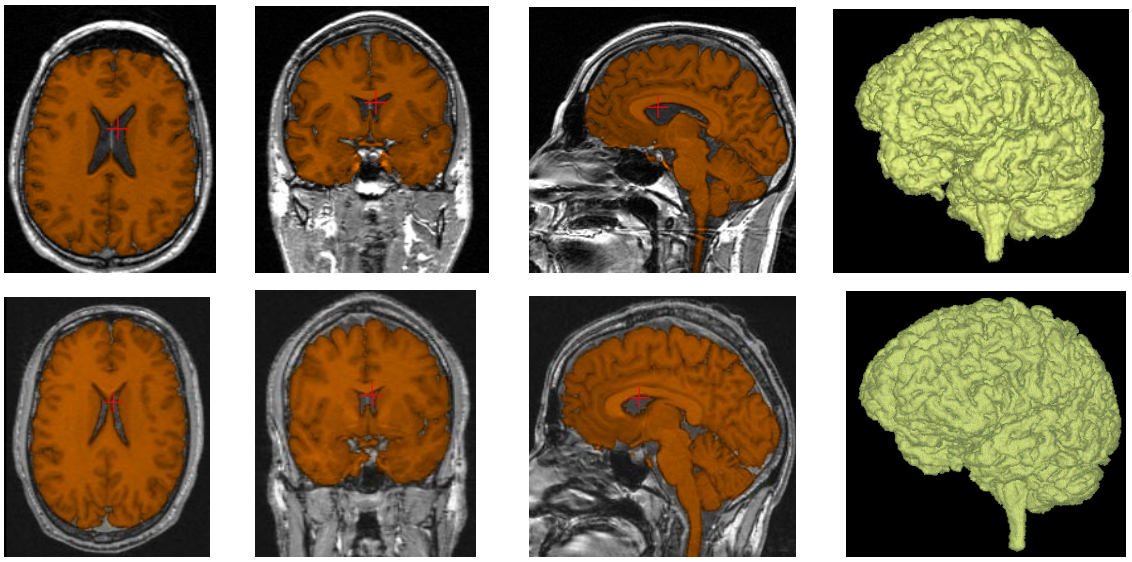

Figure 4: *Brain segmentation (orange) for two different subjects (initialization with a cube of size* $40 \times 80 \times 80$ *located inside the brain). The first three columns respectively show axial, coronal and saggital planes, the last column shows 3-D views of the segmented brains.*

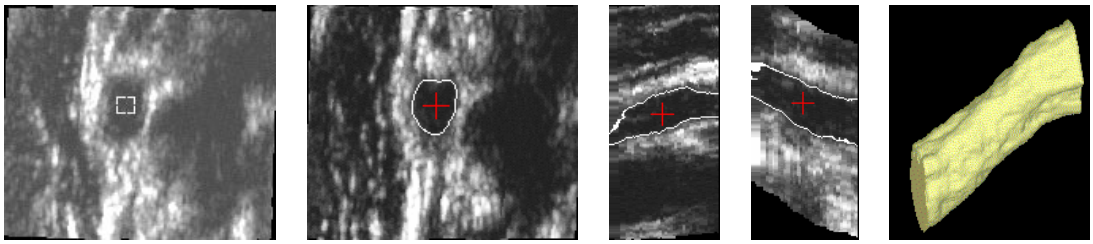

(a) (b) (c) (d) (e)

Figure 5: *Segmentation result on a* $256 \times 256 \times 80$ *ultrasound image of carotid (isotropic voxels). (a): initialization of the segmentation with a* $10 \times 10 \times 25$ *cube. (b),(c),(d): Axial, coronal and saggital planes of the final segmentation. (e) 3D view of the segmented carotid.*

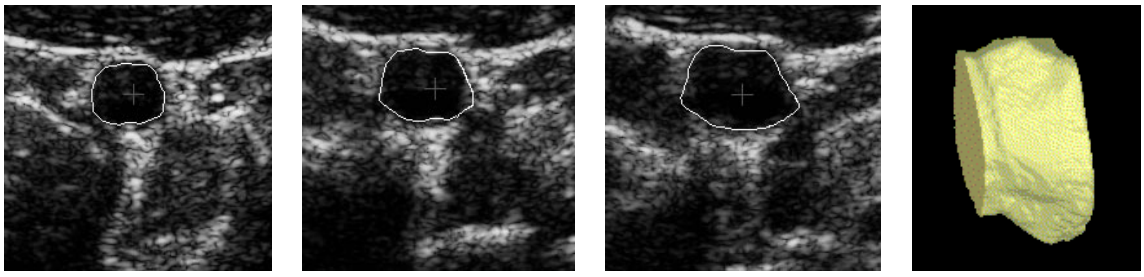

Figure 6: *Three transaxial slices and a 3D view of a segmented subpart of carotid (non isotropic voxels). The* $256 \times 256 \times 36$ *input image was initialized with a* $50 \times 50 \times 25$ *cube inside the carotid.*

6 Conclusion and further work

This paper has presented a robust evolution model for segmenting structures in 3D images using the level set formalism. It takes the statistical distributions of gray levels into a variational evolution scheme. No fine tuning of parameter is required, and good quality results have been produced on brain MRI and 3D echographies of carotid.

The accuracy of the segmentation should be further improved by extending the distribution mixture estimation to multimodal cases. This will also allow the image to be segmented into more than 2 classes. Our goal is to apply the method to various kinds of 3D images, and more especially to 3D ultrasound. Due to speckle noise, a method mixing variational and statistical models should be particularly appropriate to achieve good automatic segmentation. For this purpose, it will be necessary to involve more *a priori* information about the structure geometry.

Acknowledgements. The authors would like to thank Drs L. Pourcelot and F. Tranquart from Tours university hospital and Dr A. Fenster from RRI (London, Ontario) for providing the US data, and the GIS "Sciences de la cognition" for granting the MR acquisition project.

References

[1] O. Amadieu, E. Debreuve, M. Barlaud, and G. Aubert. Inward and outward curve evolution using level set method. In *ICIP*, Kobe, Japan, oct. 1999.

[2] V. Caselles, R. Kimmel, and G. Sapiro. Geodesic active contours. *IJCV*, 22:61–79, 1997.

[3] D.L. Collins, A.P. Zijdenbos, V. Kollokian, J.G. Sled, N.J. Kabani, C.J. Holmes, and A.C. Evans. Design and construction of a realistic digital brain phantom. *IEEE Transactions on Medical Imaging*, 17(3):463–468, June 1998.

[4] J. Gomes and O. Faugeras. Reconciling distance functions and Level-Sets. Technical Report 3666, Inria, apr. 1999.

[5] R. Kimmel, N. Kiryati, and A. Bruckstein. Analyzing and synthesizing images by evolving curves with the Osher-Sethian method. *IJCV*, 24(1):37–55, 1997.

[6] L. M. Lorigo, O. Faugeras, W. E. L. Grimson, R. Keriven, and R. Kikinis. Segmentation of bone in clinical knee MRI using texture-based geodesic active contours. In *MICCAI*, pages 1195–1204, Cambridge, MA, USA, oct. 1998.

[7] R. Malladi, J.A. Sethian, and B.C. Vemuri. Shape modeling with front propagation: A level set approach. *IEEE Tr. on PAMI*, 17(2):158–175, feb. 1995.

[8] M. Mignotte and J. Meunier. Deformable template and distribution mixture-based data modeling for the endocardial contour tracking in an echographic sequence. In *CVPR*, pages 225–230, jun. 1999.

[9] S. Osher and J.A. Sethian. Fronts propagating with curvature dependent speed: Algorithms based on Hamilton-Jacobi formulation. *J. of Computational Physics*, 79:12–49, 1988.

[10] C. Papin, P. Bouthemy, E. Mémin, and G. Rochard. Tracking and characterization of convective clouds from satellite images. In *EUMETSAT Meteo. Satellite Data Users Conf.*, Copenhague, sep. 1999.

[11] N. Paragios and R. Deriche. Unifying boundary and region-based information for geodesic active tracking. In *CVPR*, volume 2, pages 300–305, Fort Collins, Colorado, jun. 1999.

[12] P. Schroeter, J.-M. Vesin, T. Langenberger, and R. Meuli. Robust parameter estimation of intensity distributions for brain magnetic resonance images. *IEEE Tr. on PAMI*, 17(2):172–186, apr. 1998.

[13] D. Terzopoulos. Regularization of inverse visual problems involving discontinuities. *IEEE Tr. on PAMI*, 8(2):413–424, 1986.

[14] A. Yezzi, A. Tsai, and A. Willsky. Binary and ternary flows for image segmentation. In *ICIP*, Kobe, Japan, oct. 1999.

[15] X. Zeng, L.H. Staib, R.T. Schultz, H. Tagare, L. Win, and J.S. Duncan. A new approach to 3D sulcal ribbon finding from MR images. In *MICCAI*, pages 148–157, sep. 1999.